Title

Characterization of Coulomb Interactions in Electron Transport Through a Single Hetero-Helicene Molecular Junction Using Scanning Tunneling Microscopy.

Journal

Journal of Physical Chemistry A, 129(7)

Authors

Shi, Yueqing

Bi, Liya

Wang, Zihao

et al.

Publication Date

2025-02-20

DOI

10.1021/acs.jpca.4c06418

Peer reviewed

THE JOURNAL OF PHYSICAL CHEMISTRY A
A JOURNAL OF THE AMERICAN CHEMICAL SOCIETY

pubs.acs.org/JPCA
Article

Characterization of Coulomb Interactions in Electron Transport Through a Single Hetero-Helicene Molecular Junction Using Scanning Tunneling Microscopy

Published as part of The Journal of Physical Chemistry A special issue "Vicki H. Grassian Festschrift".

Yueqing Shi,[⊥] Liya Bi,[⊥] Zihao Wang,[⊥] Kangkai Liang, Ji-Kun Li, Xiao-Ye Wang, Wan-Lu Li, and Shaowei Li*

Cite This: J. Phys. Chem. A 2025, 129, 1801−1807

Read Online

ACCESS | Metrics & More | Article Recommendations | Supporting Information

ABSTRACT: Characterization of the structural and electron transport properties of single chiral molecules provides critical insights into the interplay between their electronic structure and electrochemical environments, providing broader implications given the significance of molecular chirality in chiroptical applications and pharmaceutical sciences. Here, we examined the topographic and electronic features of a recently developed chiral molecule, B,N-embedded double hetero[7]helicene, at the edge of Cu(100)-supported NaCl thin film with scanning tunneling microscopy and spectroscopy. An electron transport energy gap of 3.2 eV is measured, which is significantly larger than the energy difference between the highest occupied and the lowest unoccupied molecular orbitals given by theoretical calculations or optical measurements. Through first-principles calculations, we demonstrated that this energy discrepancy results from the Coulomb interaction between the tunneling electron and the molecule's electrons. This occurs in electron transport processes when the molecule is well decoupled from the electrodes by the insulating decoupling layers, leading to a temporary ionization of the molecule during electron tunneling. Beyond revealing properties concerning a specific molecule, our findings underscore the key role of Coulomb interactions in modulating electron transport in molecular junctions, providing insights into the interpretation of scanning tunneling spectroscopy features of molecules decoupled by insulating layers.

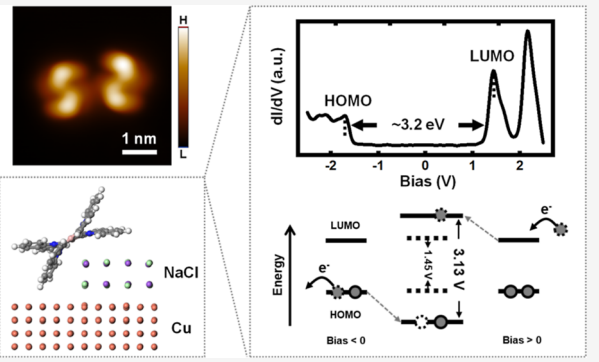

1. INTRODUCTION

Chiral luminescent materials have broad applications in optoelectronic devices such as chiral sensors and organic light-emitting diodes.[1−4] Among these materials, helicenes, a class of intrinsically chiral polycyclic aromatic hydrocarbons, have attracted considerable attention for their exceptional chiroptical properties owing to their uniquely distorted helical geometry and extended π-conjugation.[5,6] Recently synthesized B,N-embedded double hetero[7]helicenes (DH) have demonstrated impressive chiroptical properties,[7] including strong chiroptical activities from 300 to 700 nm and efficient circularly polarized luminescence from 600 to 800 nm. These excellent properties make them promising candidates for chiral optoelectronic applications in the visible and near-infrared regions. Nevertheless, this prospect is gapped by the absence of knowledge on the structural and electronic properties of DH molecules at the molecular scale.

Scanning tunneling microscope (STM) is a powerful tool for investigating the structural and electronic properties of single molecules on surfaces. It directly images the morphology and adsorption state of molecules on different surfaces.[8−10] Additionally, it can correlate the local electronic properties to the nanoscale structural features via measuring the density of states (DOS) with scanning tunneling spectroscopy (STS), which has been demonstrated for metal,[11−13] semiconductor[14,15] and molecular[16,17] systems. When directly adsorbed on metal surfaces, the electronic structures of the molecules are usually highly distorted by the electron sea underneath. However, it has been shown that the intrinsic molecular orbitals of single surface-adsorbed molecules can be preserved and surveyed with STS when an insulating film such as NaCl is added between the molecule and metal substrate.[18−24] This

Received: September 23, 2024
Revised: November 13, 2024
Accepted: November 18, 2024
Published: November 26, 2024

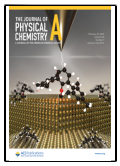

https://doi.org/10.1021/acs.jpca.4c06418
J. Phys. Chem. A 2025, 129, 1801−1807

offers an exciting platform to gain insights into the electron transport properties of the single−molecule junction consisting of a DH molecule.

In this study, we investigated individual DH molecules on both the Cu(100) surface and at the NaCl edge combining low-temperature STM measurement and density-functional theory (DFT) calculations. We characterized the electron transport from and to the frontier molecular orbitals of the DH molecule adsorbed at the NaCl edge with STS and found the measured energy gap between the highest occupied molecular orbital (HOMO) and the lowest unoccupied molecular orbital (LUMO) to be ∼1.3−1.4 eV larger than the optical gap revealed by ultraviolet−visible (UV−vis) absorption or photoluminescence (PL) measurements. Based on our DFT calculations, we assign this difference to the temporary ionization of the molecule by the tunneling electron, which increases the measured transport gap to account for the additional Coulomb repulsion/attraction energy required for an electron to tunnel into/out from the molecular orbitals. This additional energy is only observed when the molecule is strongly decoupled from the Cu surface by a NaCl thin film and is absent when the molecule is more weakly decoupled, such as when bound to a defect site on the NaCl island.

2. METHODS

2.1. Sample Preparation. The DH molecules were synthesized and characterized according to previously published procedures.[7] The thermogravimetric analysis plot of the DH powder (Figure S1) shows an onset evaporation temperature of ∼470 °C in the N_2 atmosphere. Therefore, we prepared the surface-adsorbed DH sample in the ultrahigh vacuum (UHV) chambers using the following procedures. First, we cleaned the single-crystal Cu(100) substrate with cycles of successive Ar^+ sputtering and thermal annealing. Then, scattered NaCl islands were grown on the room-temperature Cu(100) surface via thermally sublimating NaCl crystals with a homemade Knudsen cell evaporator. These NaCl flakes are terminated with (100) facet and predominantly bilayers as reported by many studies,[25,26] which are also shown in Figure S2. Afterward, the as-prepared NaCl/Cu(100) substrate was cooled down by transferring it into the ∼5 K STM junction. Finally, we dosed submonolayer DH molecules onto the cold NaCl/Cu(100) surface again by thermal sublimation with another homemade Knudsen cell evaporator. In the final step, we had to open the front door on the thermal shielding of the STM junction to directly expose the NaCl/Cu(100) surface to the DH molecular beam, which inevitably warmed up the substrate surface and might have induced the surface diffusion of DH molecules.

2.2. STM and STS Characterizations. STM and STS measurements were conducted with a customized CreaTec low-temperature STM operating at ∼5 K and a base pressure of $<1 \times 10^{-10}$ Torr. The electrochemically etched W tips were used for all data acquisition. They were first cleaned and sharpened by Ar^+ sputtering and thermal annealing, and further conditioned by repeatedly poking on the Cu(100) surface until single-molecule resolution was achieved. The STM or topographic images were taken under the constant current mode by recording z with the feedback on. The STS or dI/dV spectra were acquired by recording the first harmonic output of a lock-in amplifier while sweeping the bias. The modulation on the sample bias was 10 mV (root-mean-square) at a frequency of 977 Hz and the feedback was off while bias sweeping. All bias voltages refer to the sample voltage with respect to the tip.

2.3. PL and UV−Vis Absorption Measurements. PL spectra and UV−vis absorption spectra were recorded by the SpectraMax iD5 multimode readers. A 350 nm light source was used for excitation in the PL measurements. The DH molecules were dissolved in the toluene (1.5×10^{-5} M).

2.4. First-Principles Calculations. The Vienna ab initio simulation package[27−29] was used for geometry optimization and electronic property calculation with the projector augmented wave method.[30] The exchange−correlation energy was described by the generalized gradient approximation in the form proposed by Perdew−Burke−Ernzerhof.[31,32] The Cu(100) surface was simulated by a $6 \times 6 \times 1$ supercell with a thickness of 4 layers. To model the bilayer NaCl island on Cu(100), a $4 \times 4 \times 1$ NaCl supercell was added to the Cu supercell by aligning NaCl[100] with Cu[100] and placing one Cl atom on a top site of the Cu surface. This compression represents a NaCl/Cu lattice parameter matching of 2:3, the same as previous studies.[33,34] The NaCl edge was then built from the optimized bilayer NaCl on Cu(100) by cutting the NaCl lattice along its (010) plane. There are two possible configurations of NaCl edges, type I and type II (shown in Figure S3). The type I edge of bilayer NaCl was chosen to simulate the molecular adsorption configuration. A vacuum of at least 20 Å was added along the z-axis to prevent spurious interactions with the neighboring cells.

The cutoff energy for the plane wave basis set was set to 600 eV for all calculations. A Γ-centered Monkhorst−Pack k-point mesh was adopted for the Brillouin-zone integration. The van der Waals interactions were evaluated by DFT-D3[35] method with the Becke-Johnson damping function[36] in all calculations. The blocked-Davidson algorithm was used for electronic Hamiltonian matrix diagonalization.[28,29] The convergence criterion for electronic self-consistent loops was set to 10^{-5} eV. All structures were relaxed until the Hellmann−Feynman forces on each atom were less than 10^{-2} eV/Å. The attribution of electronic eigenstates is determined by the sum of the projections of the wave function on all single atomic orbitals of atoms in each part of the model. The adsorption energies, E_{ads}, were calculated by subtracting the sum of the substrate [Cu(100) or NaCl/Cu(100)] energy, E_{sub}, and a gas-phase DH molecule energy, E_{mol}, from the total energy of the relaxed molecule−substrate system, E_{tot}. That is

$$E_{ads} = E_{tot} - E_{sub} - E_{mol}$$

3. RESULTS AND DISCUSSION

The top panels in Figure 1a depict the molecular structures of both enantiomers, namely, left-handed (L-) and right-handed (R-) DH molecules. The racemates of DH molecules were sublimated (Figure S1) onto the substrate surface in the UHV chamber as detailed in Supporting Information. Shown in Figure 1b is the STM image of a pair of mirror-symmetric molecules on the bare Cu(100) surface. We assigned the molecule that has a contour resembling the letter S to L-DH (left in Figure 1b) and the other one to R-DH (right in Figure 1b) according to their 3D structures in Figure 1a. In other words, when adsorbed on Cu(100), the DH molecules mainly adopt a geometry that is overall parallel to the surface (Figure 1a, bottom panels), as supported by the DFT-calculated adsorption geometry of an R-DH molecule on Cu(100) (Figure S4). The fact that DH molecules are stably adsorbed

https://doi.org/10.1021/acs.jpca.4c06418
J. Phys. Chem. A 2025, 129, 1801−1807

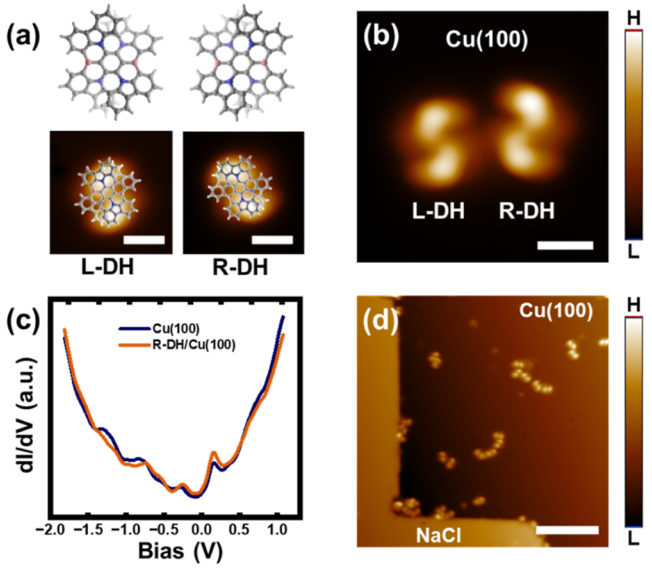

Figure 1. Adsorption of DH molecules on Cu(100). (a) Top panels: top view of the 3D structures of the DH molecules with both chirality, i.e., L- and R-. The C, N, and B atoms are shown in gray, blue, and red. The color gradient represents the relative vertical positions of the atoms. Darker color corresponds to higher *z*. Bottom panels: STM images of individual DH molecules with their molecular structures overlaid. Scale bar = 1 nm. (b) Topographic image of a pair of L- and R-DH molecules adsorbed on Cu(100) (scale bar = 1 nm). Imaging parameters were set to 500 mV, 30 pA. (c) STS spectra of an R-DH molecule on Cu(100) (orange) and the substrate (blue). The tunneling gaps were set to −2 V and 3 nA. (d) Large-area scan of the DH molecules on surfaces. Scale bar = 10 nm. Imaging parameters were set to 500 mV, 20 pA.

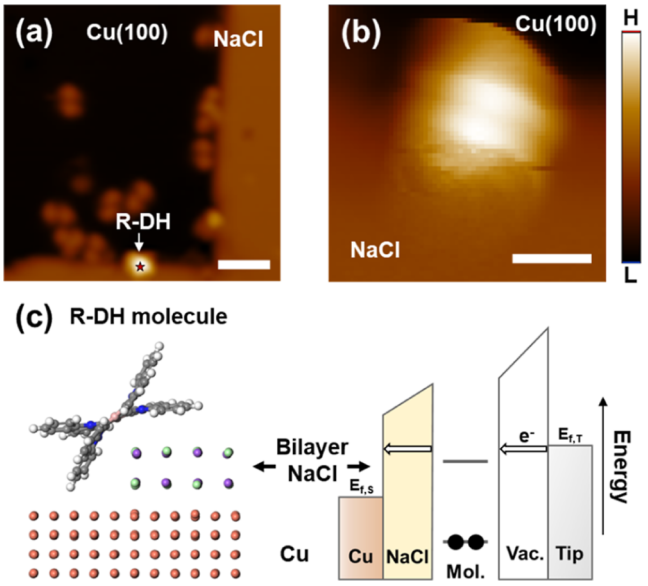

Figure 2. Adsorption of DH molecules at the edge of NaCl/Cu(100). (a) STM image of DH molecules on Cu(100) and an R-DH molecule at the NaCl edge. Scale bar = 3 nm. (b) Zoom-in image of the R-DH molecule in (a). Scale bar = 1 nm. Imaging parameters were set to (a) 800 mV, 7 pA and (b) 1.65 V, 7 pA. (c) Left: side view of the DFT-calculated adsorption geometry of an R-DH molecule at the NaCl edge. Right: schematic representation of electron transport through the adsorbed DH molecule in the double−barrier junction at positive bias.

indicates a substantial orbital hybridization with the metal substrate. This is supported by the STS measurements showing that the DOS of an R-DH molecule adsorbed on Cu(100) is nearly identical to that of the substrate (Figure 1c).

Thin-layer NaCl has been widely utilized to disentangle the molecules from the metal substrates for characterizing the molecular electronic structure with STS.[18,21,37] When inspecting the surface, we found that DH molecules predominantly stayed on the bare Cu(100) areas and occasionally came across DH molecules that were adsorbed at the edges of NaCl thin films (Figures 1d and 2a), but never observed a DH molecule on the NaCl terraces even with a very heavy molecular dosage. This finding indicates negligible binding of DH molecules to the NaCl/Cu(100) surface, which leads to unstable molecular adsorption even at such a low temperature. Our DFT calculations well reproduced this and revealed an adsorption energy of −1.04 eV when an R-DH molecule binds to Cu(100), as compared to only −0.28 eV on NaCl/Cu(100) (Figure S4). To investigate the electronic properties of DH molecules, we focused on the DH molecules that resided at the NaCl edges. Figure 2b shows the zoom-in image of such an R-DH molecule, whose chirality was confirmed by pushing it to the adjacent Cu(100) surface with the STM tip after all measurements (Figure S5). According to the DFT calculations, the R-DH molecule covers the NaCl edge with an ∼2.5 Å gap between the lowest H atom and the surface Cu atom (Figure 2c, left).

When sandwiched in between the STM tip and NaCl/Cu(100) surface, the DH molecule is effectively in a double-barrier tunnel junction as sketched in the right panel of Figure 2c. Figure 3a showcases a representative STS spectrum taken over the R-DH molecule in Figure 2b. A HOMO−LUMO gap of ∼3.2 eV was clearly resolved and is consistent with the effective decoupling of the molecule from Cu(100) surface as captured by the theory (Figure 2c, left). No obvious difference in electronic structure is resolved between molecules with different chirality. Small variation in spectrum features in dI/dV is observed among molecules adsorbed at different sites, likely due to the inhomogeneity in local chemical environment. Notably, the HOMO−LUMO gap of the single surface-adsorbed DH molecule measured with STS is significantly larger than the optical gap, ∼ 1.87−1.97 eV, as deduced from the UV−vis (Figure 3b) or PL (Figure 3c) spectra of racemic DH molecules dissolved in toluene. It is also worth noting that the HOMO in the dI/dV spectrum exhibits a double peak with an energy separation of approximately 150 meV. This feature, while captured in UV−vis (Figure 3b) and PL (Figure 3c) spectra, was not captured by our DFT calculations (Figure 4a). This double peak may result from the further broken of molecular inversion symmetry upon surface adsorption, in conjunction with the lifting of spin degeneracy in HOMO due to spin−orbit coupling, a phenomenon that is challenging to simulate accurately with the DFT package we employed.

To explain the significant difference between the HOMO−LUMO gap observed in STS and optical studies, it is important to consider the temporary ionization of the molecule during electron transport which is absent in optical excitation processes. Usually, the measured gaps from both electron transport and optical excitation are deviated from the intrinsic energy difference between HOMO and LUMO. The gap observed in STS could be wider than the actual gap because it reflects the transiently charged state of the molecule, requiring consideration of the internal electrostatic potential.[20,38] In

https://doi.org/10.1021/acs.jpca.4c06418
J. Phys. Chem. A 2025, 129, 1801−1807

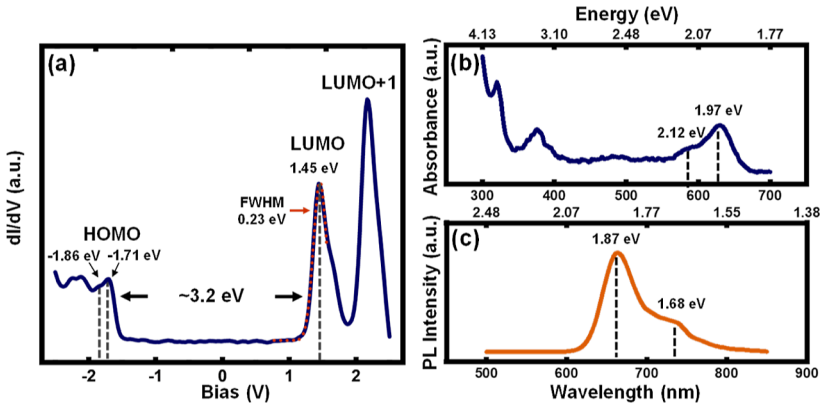

Figure 3. Characterizing the electronic structures of DH molecules. (a) STS spectrum of an R-DH molecule at the NaCl edge. The tunneling gap was set to 2.5 V and 100 pA. The red dotted line is a Gaussian fit for LUMO. (b) UV−vis absorption and (c) PL spectra of the racemic DH molecules in toluene.

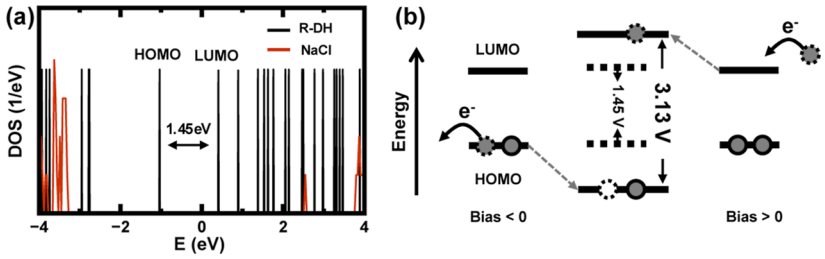

Figure 4. Computational insights into the HOMO−LUMO gap of single surface-adsorbed R-DH molecule during electron transport. (a) DFT-calculated DOS of the R-DH molecule at the NaCl edge (black) and the bilayer NaCl (red). (b) Schematics showing the broadened HOMO−LUMO gap after considering the on-site Coulomb interactions due to the temporary charging of an R-DH molecule in the STS measurements.

contrast, the optical gap could be narrower than the fundamental gap owing to the attractive Coulomb interaction within the electron−hole pair or the exciton binding energy upon optically exciting the molecules. Therefore, both the widening of the HOMO−LUMO gap and the narrowing of the optical gap could contribute to the observed ∼1.3−1.4 eV difference between them. However, we propose that the broadened HOMO−LUMO gap is the primary contributor to this significant energy difference since the exciton binding energy in most helicenes has been reported to be less than 0.5 eV.[39−41] Specifically, when measuring the molecular orbitals on NaCl/Cu(100) with STS, the molecule is temporarily charged due to the weak hybridization with the metal substrate with the insulating layer in between, leading to a prolonged lifetime of the charged states up to tens of nanoseconds.[37] The localized electron/hole on the LUMO/HOMO for a closed shell molecule like DH will thus transiently lift/lower the corresponding orbital because of the Coulomb energy involved in adding/removing an electron to/from the molecule, leading to an enlarged HOMO−LUMO gap. We note that spectroscopic features associated with doubly charged states were not observed during the experiment, indicating that the molecule relaxes to the neutral state before the arrival of a second tunneling electron.

This proposed mechanism is corroborated by further DFT calculations. The calculated DOS of a neutral R-DH molecule at the NaCl edge reveals a HOMO−LUMO gap of 1.45 eV (Figure 4a), which is only slightly larger than that of a gas-phase molecule (Figure S6), indicating negligible orbital perturbation from both NaCl and Cu. To accurately model the electron transport processes within the junction during STS measurement, the ionization of the molecule is incorporated into calculations, which include the interaction terms for electron tunneling into or out of the molecular orbitals. The energy level for LUMO tunneling is computed using self-consistent charge density, accounting for repulsive Coulomb interactions between the tunneling electron (into LUMO) and the occupied orbitals. A similar analysis is applied to the HOMO, where the interaction term becomes attractive after electron tunneling. The HOMO−LUMO gap is determined through partial-occupancy calculations with fixed self-consistent wave functions. After factoring in Coulomb repulsion and attraction during tunneling, the gap enlarges by 1.68 eV resulting from shifts in the LUMO and HOMO (Figure 4b), aligning with the ∼1.3−1.4 eV difference between the STS and optical gaps of the DH molecule.

Additionally, the enlargement of the HOMO−LUMO gap in STS measurement is absent when the molecule is bound to a defect site at the edge of the NaCl island (Figure 5, left inset), where the molecule−substrate hybridization is stronger than at the intact NaCl edge (Figure 2b,c) but still much weaker than for molecules directly adsorbed on the Cu surface. In this case, STS resolves the LUMO and HOMO at 1.15 eV and −1.45 eV, respectively, corresponding to a ∼ 2.6 eV gap, which is much closer to that derived from the optical measurements as compared to the gap for molecules adsorbed at the intact NaCl edge. The weak conductance features observed between −1.2 and 0 V bias are assigned to the Cu surface states by comparing with the dI/dV of bare Cu surface (Figure 1c). Besides, both the LUMO and HOMO peaks in the STS measured at the defect site are broadened, with long tails in the dI/dV signal extending across the Fermi level. The full width at half-

https://doi.org/10.1021/acs.jpca.4c06418
J. Phys. Chem. A 2025, 129, 1801−1807

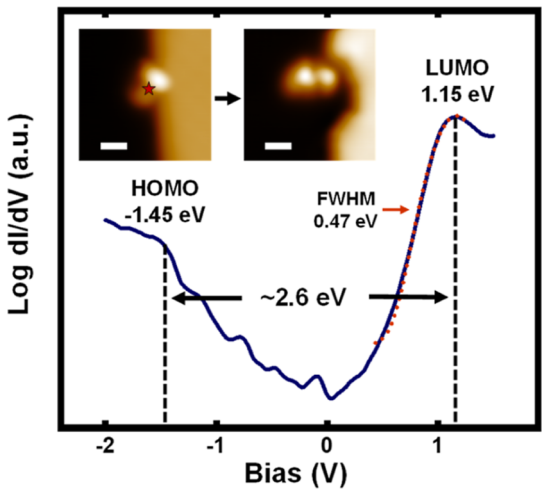

Figure 5. STS spectrum of an L-DH molecule at the NaCl edge defect (insets) plotted in the log scale. The red dotted line is a Gaussian fit for LUMO. The tunneling gap was set to −2 V and 300 pA. The right inset shows the same molecule in the left one after being pushed to Cu(100) by the STM tip. Scale bar = 1 nm. Imaging parameters were set to −1.14 V, 30 pA (left inset) and −1 V, 30 pA (right inset). The small dI/dV features between −1.2 and 0.5 V are also observed in the STS of bare Cu surface, and are assigned as the surface states of Cu.

maximum for the LUMO peak of the molecule at the intact NaCl edge is ∼0.23 eV (Figure 3a), about half that of the molecule bound to the defect (Figure 5). This broadening results from the hybridization of discrete molecular orbitals with the continuum metal states of the substrate, creating a tunneling channel through which the incoming electron quickly leaves the molecule, exchanging energy directly with the Cu lattice. As a result, the Coulomb interaction does not obviously influence the tunneling process.

4. CONCLUSIONS

In this study, we characterized the structural and electronic properties of a single DH molecule in a double-barrier tunneling junction formed between the STM tip and a NaCl thin film supported by Cu(100) substrate. The chirality of the molecule is easily identifiable in topographic images when it is adsorbed directly on Cu(100). We found that DH molecules tend to avoid adsorption on the terrace of bilayer NaCl but can weakly bond to the edge of the NaCl island. The weak molecule−bath interaction extends the lifetime of the charged states, leading to the temporary ionization of the molecule during the STS measurement. Consequently, the measured HOMO−LUMO gap in STS is significantly broader for the molecules at the NaCl edge due to the Coulomb interaction that the tunneling electrons experience when passing through the molecule. This effect is absent in the molecule adsorbed on the defect sites of NaCl, where the molecule−substrate hybridization is enhanced. Our study provides molecular-scale insights into the electron transport properties of single DH molecules in an STM junction and highlights how they are influenced by molecule−substrate hybridization.

■ ASSOCIATED CONTENT

Supporting Information

The Supporting Information is available free of charge at https://pubs.acs.org/doi/10.1021/acs.jpca.4c06418.

Thermogravimetric analysis of racemic DH powder; height information for bilayer NaCl; two possible NaCl edge configurations on Cu(100); DFT-calculated adsorption geometries of individual R-DH molecule on different surfaces; STM images of an R-DH molecule before and after being pushed to the Cu(100) surface; DFT-calculated DOS of the gas-phase R-DH molecule (PDF)

■ AUTHOR INFORMATION

Corresponding Author

Shaowei Li − *Department of Chemistry and Biochemistry, University of California, San Diego, La Jolla, California 92093-0309, United States; Program in Materials Science and Engineering, University of California, San Diego, La Jolla, California 92093-0418, United States;* orcid.org/0000-0002-4627-626X; Email: shaoweili@ucsd.edu

Authors

Yueqing Shi − *Department of Chemistry and Biochemistry, University of California, San Diego, La Jolla, California 92093-0309, United States*

Liya Bi − *Department of Chemistry and Biochemistry, University of California, San Diego, La Jolla, California 92093-0309, United States; Program in Materials Science and Engineering, University of California, San Diego, La Jolla, California 92093-0418, United States;* orcid.org/0009-0009-3041-2771

Zihao Wang − *Department of Chemistry and Biochemistry, University of California, San Diego, La Jolla, California 92093-0309, United States; Program in Materials Science and Engineering, University of California, San Diego, La Jolla, California 92093-0418, United States*

Kangkai Liang − *Department of Chemistry and Biochemistry, University of California, San Diego, La Jolla, California 92093-0309, United States; Program in Materials Science and Engineering, University of California, San Diego, La Jolla, California 92093-0418, United States*

Ji-Kun Li − *State Key Laboratory of Elemento-Organic Chemistry, College of Chemistry, Nankai University, Tianjin 300071, China*

Xiao-Ye Wang − *State Key Laboratory of Elemento-Organic Chemistry, College of Chemistry, Nankai University, Tianjin 300071, China;* orcid.org/0000-0003-3540-0277

Wan-Lu Li − *Program in Materials Science and Engineering, University of California, San Diego, La Jolla, California 92093-0418, United States; Aiiso Yufeng Li Family Department of Chemical and Nano Engineering, University of California, San Diego, La Jolla, California 92093-0448, United States;* orcid.org/0000-0003-0098-0670

Complete contact information is available at: https://pubs.acs.org/10.1021/acs.jpca.4c06418

Author Contributions

⊥Y.S., L.B., and Z.W. have contributed equally to this work.

Notes

The authors declare no competing financial interest.

■ ACKNOWLEDGMENTS

This work was supported by the United States National Science Foundation (NSF) under grant no. CHE-2303936 (to Shaowei Li). The authors acknowledge the use of facilities and

instrumentation supported by NSF through the UC San Diego Materials Research Science and Engineering Center (UCSD MRSEC) with grant no. DMR-2011924. This work used the San Diego Supercomputer Center (SDSC) Expanse at UC San Diego for theoretical calculations through allocation CHE-240050 from the Advanced Cyberinfrastructure Coordination Ecosystem: Services & Support (ACCESS) program, which is supported by NSF grants nos. OAC-2138259, OAC-2138286, OAC-2138307, OAC-2137603, and OAC-2138296.

REFERENCES

(1) Furlan, F.; Moreno-Naranjo, J. M.; Gasparini, N.; Feldmann, S.; Wade, J.; Fuchter, M. J. Chiral materials and mechanisms for circularly polarized light-emitting diodes. *Nat. Photonics* **2024**, *18* (7), 658−668.
(2) Wang, Z.; Cheng, F.; Winsor, T.; Liu, Y. Optical chiral metamaterials: a review of the fundamentals, fabrication methods and applications. *Nanotechnology* **2016**, *27* (41), 412001.
(3) Niu, X.; Zhao, R.; Yan, S.; Pang, Z.; Li, H.; Yang, X.; Wang, K. Chiral Materials: Progress, Applications, and Prospects. *Small* **2023**, *19* (38), No. e2303059.
(4) Niu, X.; Yang, X.; Li, H.; Liu, J.; Liu, Z.; Wang, K. Application of chiral materials in electrochemical sensors. *Mikrochim. Acta* **2020**, *187* (12), 676.
(5) Meng, G.; Zhou, J.; Han, X. S.; Zhao, W.; Zhang, Y.; Li, M.; Chen, C. F.; Zhang, D.; Duan, L. B-N Covalent Bond Embedded Double Hetero-[n]helicenes for Pure Red Narrowband Circularly Polarized Electroluminescence with High Efficiency and Stability. *Adv. Mater.* **2024**, *36* (5), No. e2307420.
(6) Guo, W. C.; Zhao, W. L.; Tan, K. K.; Li, M.; Chen, C. F. B,N-Embedded Hetero[9]helicene Toward Highly Efficient Circularly Polarized Electroluminescence. *Angew. Chem., Int. Ed. Engl.* **2024**, *63* (18), No. e202401835.
(7) Li, J. K.; Chen, X. Y.; Guo, Y. L.; Wang, X. C.; Sue, A. C.; Cao, X. Y.; Wang, X. Y. B,N-Embedded Double Hetero[7]helicenes with Strong Chiroptical Responses in the Visible Light Region. *J. Am. Chem. Soc.* **2021**, *143* (43), 17958−17963.
(8) Anirban, A. 40 years of scanning tunnelling microscopy. *Nat. Rev. Phys.* **2022**, *4* (5), 291.
(9) Binnig, G.; Rohrer, H.; Gerber, C.; Weibel, E. 7 × 7 Reconstruction on Si(111) Resolved in Real Space. *Phys. Rev. Lett.* **1983**, *50* (2), 120−123.
(10) Binnig, G.; Rohrer, H. Scanning tunneling microscopy—from birth to adolescence. *Rev. Mod. Phys.* **1987**, *59* (3), 615−625.
(11) Sugimoto, A.; Ishimitsu, S.; Ohtsubo, H.; Matsumoto, K.; Saito, T.; Ekino, T.; Gabovich, A. M. STM/STS study of the local density of states in Cu doped Fe(Se,Te) superconductors. *J. Phys.: Conf. Ser.* **2022**, *2323* (1), 012010.
(12) Starfelt, S.; Johansson, L. S. O.; Zhang, H. M. STM/STS and photoemission study of Ag thin films on Ga/Si(111) (3 × 3)R30. *Surf. Sci.* **2019**, *682*, 25−32.
(13) Yu, A.; Li, S.; Czap, G.; Ho, W. Tunneling-Electron-Induced Light Emission from Single Gold Nanoclusters. *Nano Lett.* **2016**, *16* (9), 5433−5436.
(14) Peng, W.; Wang, H.; Lu, H.; Yin, L.; Wang, Y.; Grandidier, B.; Yang, D.; Pi, X. Recent Progress on the Scanning Tunneling Microscopy and Spectroscopy Study of Semiconductor Heterojunctions. *Small* **2021**, *17* (50), No. e2100655.
(15) Große, C.; Gunnarsson, O.; Merino, P.; Kuhnke, K.; Kern, K. Nanoscale Imaging of Charge Carrier and Exciton Trapping at Structural Defects in Organic Semiconductors. *Nano Lett.* **2016**, *16* (3), 2084−2089.
(16) Yu, A.; Li, S.; Wang, H.; Chen, S.; Wu, R.; Ho, W. Visualization of Nanoplasmonic Coupling to Molecular Orbital in Light Emission Induced by Tunneling Electrons. *Nano Lett.* **2018**, *18* (5), 3076−3080.
(17) You, S.; Yu, C.; Gao, Y.; Li, X.; Peng, G.; Niu, K.; Xi, J.; Xu, C.; Du, S.; Li, X.; Yang, J.; Chi, L. Quantifying the conductivity of a single polyene chain by lifting with an STM tip. *Nat. Commun.* **2024**, *15* (1), 6475.
(18) Repp, J.; Meyer, G.; Stojkovic, S. M.; Gourdon, A.; Joachim, C. Molecules on insulating films: scanning-tunneling microscopy imaging of individual molecular orbitals. *Phys. Rev. Lett.* **2005**, *94* (2), 026803.
(19) Repp, J.; Meyer, G. Scanning tunneling spectroscopy of molecules on insulating films. *Chimia (Aarau)* **2010**, *64* (6), 370−375.
(20) Wu, S. W.; Nazin, G. V.; Chen, X.; Qiu, X. H.; Ho, W. Control of relative tunneling rates in single molecule bipolar electron transport. *Phys. Rev. Lett.* **2004**, *93* (23), 236802.
(21) Repp, J.; Meyer, G. Scanning tunneling microscopy of adsorbates on insulating films. From the imaging of individual molecular orbitals to the manipulation of the charge state. *Appl. Phys. A: Mater. Sci. Process.* **2006**, *85* (4), 399−406.
(22) Miwa, K.; Imada, H.; Imai-Imada, M.; Kimura, K.; Galperin, M.; Kim, Y. Many-Body State Description of Single-Molecule Electroluminescence Driven by a Scanning Tunneling Microscope. *Nano Lett.* **2019**, *19* (5), 2803−2811.
(23) Imai-Imada, M.; Imada, H.; Miwa, K.; Jung, J.; Shimizu, T. K.; Kawai, M.; Kim, Y. Energy-level alignment of a single molecule on ultrathin insulating film. *Phys. Rev. B* **2018**, *98* (20), 201403.
(24) Grewal, A.; Leon, C. C.; Kuhnke, K.; Kern, K.; Gunnarsson, O. Character of Electronic States in the Transport Gap of Molecules on Surfaces. *ACS Nano* **2023**, *17* (14), 13176−13184.
(25) Guo, Q.; Qin, Z.; Liu, C.; Zang, K.; Yu, Y.; Cao, G. Bias dependence of apparent layer thickness and Moiré pattern on NaCl/Cu(001). *Surf. Sci.* **2010**, *604* (19−20), 1820−1824.
(26) Guo, Q. M.; Qin, Z. H.; Huang, M.; Mantsevich, V. N.; Cao, G. Y. Image potential states mediated STM imaging of cobalt phthalocyanine on NaCl/Cu(100). *Chinese Physics B* **2016**, *25* (3), 036801.
(27) Kresse, G.; Hafner, J. Ab initio molecular dynamics for liquid metals. *Phys. Rev. B* **1993**, *47* (1), 558−561.
(28) Kresse, G.; Furthmüller, J. Efficient iterative schemes for ab initio total-energy calculations using a plane-wave basis set. *Phys. Rev. B* **1996**, *54* (16), 11169−11186.
(29) Kresse, G.; Furthmüller, J. Efficiency of ab-initio total energy calculations for metals and semiconductors using a plane-wave basis set. *Comput. Mater. Sci.* **1996**, *6* (1), 15−50.
(30) Blöchl, P. E. Projector augmented-wave method. *Phys. Rev. B* **1994**, *50* (24), 17953−17979.
(31) Perdew, J. P.; Burke, K.; Ernzerhof, M. Generalized Gradient Approximation Made Simple. *Phys. Rev. Lett.* **1996**, *77* (18), 3865−3868.
(32) Kresse, G.; Joubert, D. From ultrasoft pseudopotentials to the projector augmented-wave method. *Phys. Rev. B* **1999**, *59* (3), 1758−1775.
(33) Robledo, M.; Pacchioni, G.; Martín, F.; Alcamí, M.; Díaz-Tendero, S. Adsorption of Benzene on Cu(100) and on Cu(100) Covered with an Ultrathin NaCl Film: Molecule−Substrate Interaction and Decoupling. *J. Phys. Chem. C* **2015**, *119* (8), 4062−4071.
(34) Robledo, M.; Díaz-Tendero, S. Exploring the Adsorption and the Potential Energy Surface of Acrylonitrile on Cu(100) and Cu(100) Coated with NaCl Layers. *J. Phys. Chem. C* **2015**, *119* (27), 15125−15136.
(35) Grimme, S.; Antony, J.; Ehrlich, S.; Krieg, H. A consistent and accurate ab initio parametrization of density functional dispersion correction (DFT-D) for the 94 elements H-Pu. *J. Chem. Phys.* **2010**, *132* (15), 154104.
(36) Grimme, S.; Ehrlich, S.; Goerigk, L. Effect of the damping function in dispersion corrected density functional theory. *J. Comput. Chem.* **2011**, *32* (7), 1456−1465.
(37) Kaiser, K.; Lieske, L. A.; Repp, J.; Gross, L. Charge-state lifetimes of single molecules on few monolayers of NaCl. *Nat. Commun.* **2023**, *14* (1), 4988.

(38) Imai-Imada, M.; Imada, H.; Miwa, K.; Jung, J.; Shimizu, T. K.; Kawai, M.; Kim, Y. Energy-level alignment of a single molecule on ultrathin insulating film. *Phys. Rev. B* **2018**, *98* (20), 201403.
(39) Hamrouni, K.; Hafedh, N.; Chmeck, M.; Aloui, F. Photo-oxidation pathway providing 15-bromo-7-cyano[6]helicene. Chiroptical and photophysical properties and theoretical investigation. *J. Mol. Struct.* **2020**, *1217*, 128399.
(40) Raouafi, S.; Aloui, F.; Hafedh, N. Synthesis, characterization, and photophysical properties of a new pentacyclic helicene. *C. R. Chim.* **2017**, *20* (11−12), 1047−1052.
(41) Bock, H.; Subervie, D.; Mathey, P.; Pradhan, A.; Sarkar, P.; Dechambenoit, P.; Hillard, E. A.; Durola, F. Helicenes from diarylmaleimides. *Org. Lett.* **2014**, *16* (6), 1546−1549.

https://doi.org/10.1021/acs.jpca.4c06418
J. Phys. Chem. A 2025, 129, 1801−1807